

Domain walls and macroscopic spin-flip-like metamagnetism in $\text{Gd}_x\text{Co}_{1-x}/\text{Gd}_y\text{Co}_{1-y}$ exchange-coupled double layers

R. Morales, J. I. Martín,* and J. M. Alameda

Departamento de Física, Universidad de Oviedo, c/ Calvo Sotelo, s/n, 33007 Oviedo, Spain

(Received 19 May 2004; revised manuscript received 11 August 2004; published 18 November 2004)

Amorphous ferrimagnetic $\text{Gd}_x\text{Co}_{1-x}/\text{Gd}_y\text{Co}_{1-y}$ exchange coupled double layers (ECDL) have been prepared in order to investigate the magnetization reversal processes and the presence of stable magnetic configurations when the chemical compositions of both layers are very similar. The ECDL samples have been grown by co-sputtering from independent pure Co and Gd targets, being 100 nm the thickness of each layer. The measurements have been done by the magneto-optical Kerr effect at both sides of the ECDL in the temperature interval 200 K–450 K, and the compositions of the two layers are $x=0.22$ and $y=0.24$. A rich variety of behaviors has been found, being the most relevant of those in the temperature range between the compensation temperatures (T_{comp}) of both layers. Some of these observed behaviors include magnetization reversal by creation/annihilation of a Bloch wall across the ECDL thickness, and a macroscopic spin-flip-like metamagnetic state where the magnetic moments form a double antiferromagnetic state with the presence of an extended Neel wall when the magnetizations of both layers are similar. A temperature phase diagram for the transition fields between different magnetic states has also been deduced, being in very good agreement with the magnetic behavior observed in the whole temperature range.

DOI: 10.1103/PhysRevB.70.174440

PACS number(s): 75.70.Cn, 75.60.-d, 75.50.Gg

I. INTRODUCTION

Multilayers and superlattices constituted by magnetic layers combined or not with nonmagnetic materials have attracted much attention, both from the technological point of view as well as in the basic research field, as they can show new and interesting magnetic properties and artificially induced stable configurations of the magnetization that are absent in bulk materials or single thin films.^{1–13} Remarkable behaviors have been found in multilayers of magnetic materials with different compositions, produced by the exchange coupling interaction between the ferromagnetic and/or antiferromagnetic ordered magnetic moments of the layers at both sides of the interfaces. These rich phenomena include exchange bias effects,⁷ enhancement of the magnetization near the interfaces,⁸ the presence of inverted hysteresis loops with negative remanence,⁹ the design of synthetic antiferromagnets for spin valves,¹⁰ perpendicular magnetic anisotropy,¹¹ proximity magnetism,¹² and a variety of stable magnetic configurations at remanence with different relative angles between the magnetic moments of the coupled layers.^{12,13}

Rare earth (RE)-transition metal (TM) amorphous alloy multilayers are a family of particular interest among the different exchange coupled systems for their fundamental and applied characteristics. These alloys present an antiferromagnetic coupling between the magnetic moments of the heavy RE and TM ions; due to the different temperature dependences of both sublattices, a compensation temperature (T_{comp}) that is compositionally dependent is usually found.¹⁴ The net magnetization of these ferrimagnetic alloys is therefore aligned with either the RE or TM moments as the temperature is below or over T_{comp} (where both magnetizations cancel each other). This main basic mechanism can result in the observation of relevant magnetic properties when these

RE-TM alloys are arranged in exchange coupled multilayers,¹⁵ such as planar Bloch walls parallel to the surface and macroscopic ferrimagnet states,¹⁶ or tailorable strong perpendicular magnetic anisotropies,^{17–19} which make them very suitable for magneto-optical recording.^{19–21}

In this work, we have studied in a wide temperature range the magnetic behavior of $\text{Gd}_x\text{Co}_{1-x}/\text{Gd}_y\text{Co}_{1-y}$ exchange coupled double layers (ECDL) with similar x and y Gd contents, in order to perform a complete description of the different magnetization configuration states that can be present in this kind of system. A rich variety of behaviors of the magnetization reversal processes has been observed, which can be understood in terms of a general phase diagram that has been deduced from the detailed analysis of the system. In particular, it allows us to describe and predict the presence of a previously unreported magnetization configuration state at temperatures where the net magnetization of both amorphous alloys is similar but aligned in each layer with either the RE or TM magnetic moments. The measurements show that such a state presents the phenomenological characteristics of a macroscopic spin-flip-like metamagnetism, where each layer is divided in the plane in two symmetrical domains with opposite magnetizations and, simultaneously, the magnetization of the top and bottom halves are also antiparallel. Induced by the exchange interaction, this is a very stable state in a wide field range around remanence.

II. EXPERIMENTAL

The RE-TM amorphous alloys bilayers, $\text{Gd}_x\text{Co}_{1-x}/\text{Gd}_y\text{Co}_{1-y}$ have been obtained by dc magnetron sputtering on Corning glass substrates as reported elsewhere.²² Briefly, the alloys were deposited at an Ar pressure of 10^{-3} Torr from high purity Co and Gd targets that are symmetrically placed at an angle of 20° with respect to the

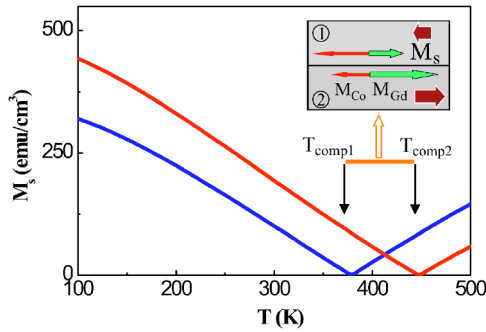


FIG. 1. (Color online) Sketch of the $M_s(T)$ curves of each layer of the $\text{Gd}_x\text{Co}_{1-x}/\text{Gd}_y\text{Co}_{1-y}$ ECDL, particularized for $x=0.22$ and $y=0.24$ values. The configuration of the magnetic moments and the magnetization of both layers in the temperature range between both compensation temperatures for $H=0$ is also represented.

normal of the substrate plane. The composition of the layers was varied by controlling the relative powers of both sputtering guns. The amorphous structure of the bilayers has been verified by x-ray diffraction. The thickness of each layer is 100 nm and the samples are *in situ* covered with a 5 nm thick layer of Mo to avoid oxidation. The magnetic characterization of the bilayers has been performed by a transverse magneto-optical Kerr effect (TMOKE),²² measuring on both sides of the samples as the substrate is transparent to visible light. Also, for the wavelength of the incident beam (670 nm and visible white light), the penetration depth of the light in these alloys can be estimated²³ to be around 40 nm, shorter than each layer thickness, and the TMOKE signal (δ_{Kerr}) is only sensitive to the magnetic behavior of the Co sublattice and not to the Gd moments contribution (then, due to the antiferromagnetic coupling between both kind of atoms, the behavior of the Gd moments configuration in each layer is deduced as the antiparallel orientation to the one measured for the Co moments).²¹ The magnetic field (H) has been applied in the sample plane along the easy axis of these uniaxial systems, that is defined by the oblique incidence of the atoms during the off-normal deposition; in particular, the easy axis is perpendicular to the plane defined by the incoming atoms.

The temperature range analyzed in the present work is mainly the interval between the two compensation temperatures in which the saturation magnetization (M_s) of both layers can become very similar at certain temperature values (see Fig. 1). In this interval the net saturation magnetization for the top layer (1) is parallel to the TM magnetic moments while, on the contrary, for the bottom layer (2) it is aligned with the RE moments, as sketched in Fig. 1 (it is the so-called type-A ECDL,²⁴ in contrast with type-P ECDL where M_s is parallel to the same kind of magnetic moment, either TM or RE, in both layers and that would correspond with $T < T_{comp1}$ or $T > T_{comp2}$). For comparison, TMOKE hysteresis loops have also been measured at temperatures where the sample is a type-P ECDL. It is worth noting that in the type-A case, when the magnetization of the sample is saturated at large enough magnetic fields, the Gd and the Co magnetic moments of one of the layers are pointing in the opposite direction to the Gd and Co moments of the other

one, so that, due to the exchange interaction at the interface of each kind of moment (especially the Co-Co one that is stronger), a 180° Bloch wall for both moments is present across the thickness in the ECDL (that is, the saturation of the sample implies the creation of a wall at the interface, while in the absence of an applied field the exchange interaction results in parallel Co and Gd moments of both layers at the interface and, therefore, in an antiparallel configuration of both spontaneous magnetizations as represented in the sketch of Fig. 1).

The compositions of the two layers in the ECDL are $x=0.22$ and $y=0.24$, respectively, as measured by x-ray microanalysis in separate single layers prepared in the same conditions. These layers present experimental $T_{comp1}=378$ K and $T_{comp2}=450$ K, in agreement with previously reported values in this composition range.¹⁴ It is worth noting that the temperature dependence of M_s for $\text{Gd}_x\text{Co}_{1-x}$ single layers with these values of Gd content and measured by vibrating sample magnetometry²² can be understood in terms of a mean-field model, with a behavior close to T_{comp} that can be described in a good approximation as M_s (emu/cm³) = $1.3(T_{comp}-T)$ for $T < T_{comp}$, and M_s (emu/cm³) = $1.05(T-T_{comp})$ for $T > T_{comp}$. Also, the coercive fields of the monolayers present a $H_c(\text{Oe})=5560/|T-T_{comp}|$ temperature dependence near T_{comp} (the coefficient indicates that the maximum value of the position gradient of the wall energy is about 17 erg/cm³).

III. RESULTS AND DISCUSSION

A. Magnetization reversal processes

Figure 2 shows the TMOKE hysteresis loops obtained by measuring from top and bottom sides of the bilayer (top and bottom pannels in all cases, respectively) illuminating the whole sample area at different representative temperatures in each significative interval. The results show a rich variety of behaviors in the magnetization reversal processes as the temperature is varied. The loop of the bottom layer presents a negative sign at saturation for every temperature, in accordance with a saturation magnetization dominated by the Gd moments and a Kerr signal that results from the Co moments contribution. On the other hand, the signal at saturation of the top layer changes from a negative to a positive sign as the temperature is increased from 370 K to 394 K crossing this layer's compensation temperature $T_{comp1}=378$ K; it corresponds to a saturation magnetization dominated by Co moments at higher temperatures and by Gd moments at lower T values. Thus, the ECDL is type P for $T < T_{comp1}$ and type A for $T > T_{comp1}$. The results show that in the type-P case ($T=370$ K) both loops present a square shape with only one jump at low fields, indicating a simultaneous switching of both magnetizations. However, at $T=394$ K, just above T_{comp1} , three jumps are observed in the top layer loop while the bottom layer one keeps its square shape. It reveals that at this temperature the reversal process of the type-A ECDL is dominated by the bottom layer magnetization that is larger than the top layer one, so that, as the field is reduced from positive to negative saturation, the top layer magnetization is

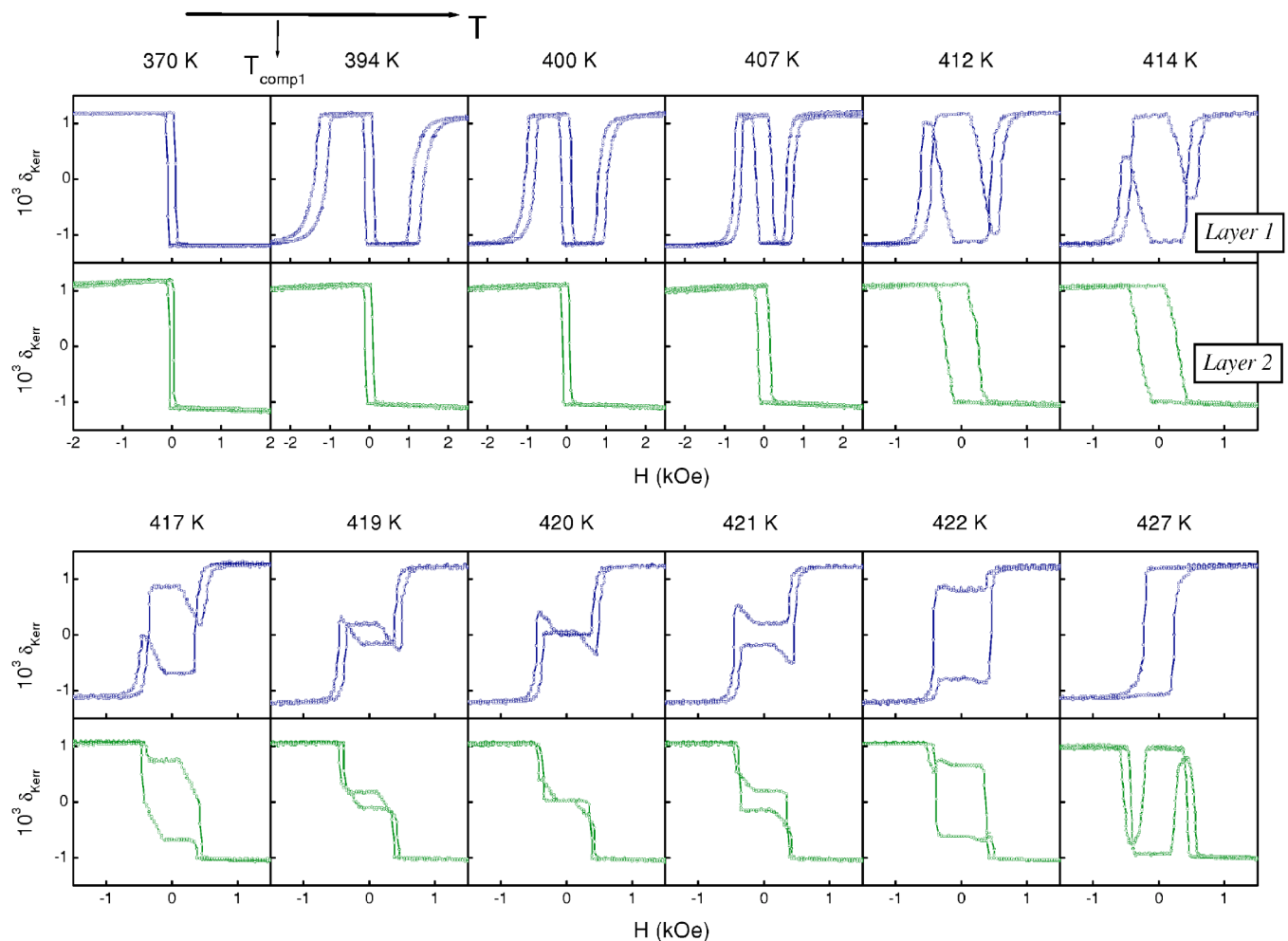


FIG. 2. (Color online) Temperature evolution of the TMOKE loops measured illuminating the whole $\text{Gd}_{0.22}\text{Co}_{0.78}/\text{Gd}_{0.24}\text{Co}_{0.76}$ ECDL from top and bottom layer sides. Only some representative loops of those measured at different temperatures are shown.

first reverted annihilating the wall across the thickness, then, both magnetizations reverse simultaneously and, finally, for more negative values, the field is intense enough to rotate again the top layer magnetization creating the wall. This kind of reversal process has been widely reported earlier both in ferrimagnetic/ferrimagnetic and ferromagnetic/ferrimagnetic coupled layers of RE-TM amorphous alloys^{16,24,25} and, in the present case, is essentially unchanged when the temperature is further increased up to 412 K. However, as the temperature increases and the compensation temperature of the bottom layer is approached its coercive field increases and by $T=414$ K it has become so large that the second jump in the top layer loop is not complete (the one associated to the simultaneous reversal of both magnetizations), as the fields at which it takes place are high enough to create at a certain value the wall across the thickness (the process associated with the third jump). The reversal processes look very different for higher temperatures, in the range 417 K–422 K; now, both loops present incomplete jumps with field intervals where the Kerr signal (and, therefore, the magnetization) remains constant. A case of particular interest is the behavior found at 420 K, where top and bottom layers show $\delta_{\text{Kerr}}=0$ in a wide field interval around $H=0$ (i.e., at remanence). For

even higher temperatures ($T=427$ K) the loops are similar to those observed previously at 412 K, but with the symmetric behavior, that is, now the reversal process is dominated by the top layer that, at these temperatures, presents a larger saturation magnetization and whose loop presents one jump while three are observed in the bottom layer measurement.

In order to understand the rich variety of behaviors observed in the TMOKE loops as a function of temperature it is necessary to consider the different possible reversal processes that can be present in the ECDL, and the energy terms associated with them. Figure 3 shows the sketches of the characteristic reversal steps, labeling the magnetic fields at which each of them takes place. The notation H_{ij}^{\pm} means the switching field at which the layer j ($=1$ or 2) reverses with the associated creation (+) or annihilation (–) of the 180° Bloch wall across the thickness. Thus, for type-P ECDL [Fig. 3(a)], the magnetization reversal between both saturation states (I and IV) can be done through different ways; in one of them, from state I the magnetization of the top layer is first reversed creating a wall across the thickness at H_{t1}^+ reaching the state II and, then, the bottom layer magnetization is reversed annihilating the wall at H_{t2}^- to get state IV. Second, it can take place along the complementary way, that

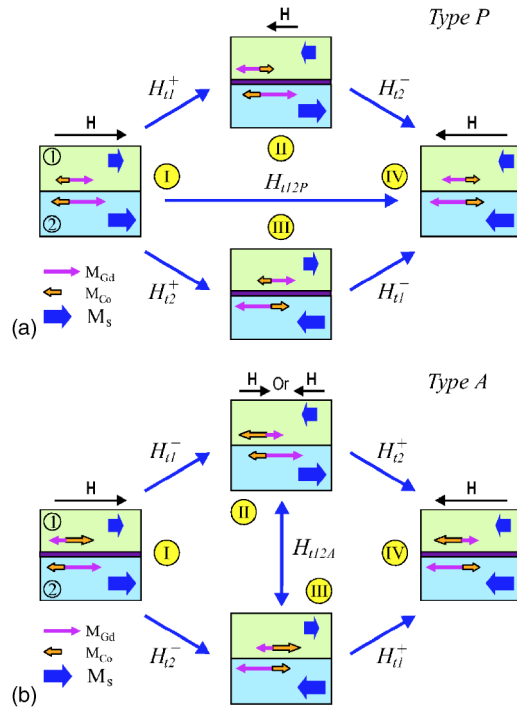


FIG. 3. (Color online) Sketches of the possible magnetization reversal processes in (a) type-P ECDL and (b) type-A ECDL. The magnetic fields associated with each step are labeled.

is, in a first step the bottom layer magnetization reverses at H_{t2}^+ reaching state III and, then, at H_{t1}^- the top magnetization is switched. Also, the magnetization of the ECDL can be directly reversed by the simultaneous switching of both individual magnetizations at H_{t12P} without creation or annihilation of the wall across the thickness. On the other hand, for a type-A ECDL [Fig. 3(b)] the reversal processes show important differences; first, the wall across the thickness between the magnetic moments present at saturation is annihilated by switching one of the individual magnetizations at either H_{t1}^- or H_{t2}^- to get states II or III, respectively; then, the opposite saturation can be reached by reversing the other magnetization creating the wall (at H_{t2}^+ or H_{t1}^+) or, also, through the simultaneous switching of both magnetizations between states II and III at H_{t12A} in a second step, that is followed by the creation of the wall (either at H_{t1}^+ or H_{t2}^+) by a new reversal of the individual layer magnetization that has already been switched initially.

B. H-T phase diagram of the switching fields

The competition between these different reversal processes sketched in Fig. 3 and their presence in the measured hysteresis loops of the ECDL can be understood by modeling the associated energy terms in a similar argumentation to that reported in Ref. 15. The Zeeman energy per unit area (E_z) of one saturated monolayer with magnetization \mathbf{M}_s under an external magnetic field \mathbf{H}_{ext} in an initial state (i) can be written as $E_{zi} = -t\mathbf{M}_{si} \cdot \mathbf{H}_{\text{ext}}$, where t is the layer thickness. Considering a uniaxial system with a field along the easy axis, if at this external field value the magnetization is just reversed,

the final state (f) has an energy $E_{zf} = -t\mathbf{M}_{sf} \cdot \mathbf{H}_{\text{ext}}$, so that $E_{zi} = E_{zf} + E_c$, where E_c is the coercive energy. As it is well known, since $\mathbf{M}_{si} = -\mathbf{M}_{sf}$ and the reversal takes place when $H_{\text{ext}} = H_c$, then $E_c = 2tM_sH_c$. In the bilayer case, the magnetization reversal of its layers can result in the creation (or annihilation) of a 180° Bloch wall across the thickness and the energy balance is modified to

$$E_{zi} = E_{zf} + E_c \pm \sigma_w, \quad (1)$$

where σ_w is the energy per unit area of the created (annihilated) wall (the positive sign corresponds with the creation and the negative sign with the annihilation). Taking \mathbf{H}_t as the field at which the magnetization of the layers is switched in the ECDL system, Eq. (1) can be written as

$$2t\mathbf{M}_{sf} \cdot \mathbf{H}_t = 2tM_sH_c \pm \sigma_w; \quad (2)$$

then, considering that H_{tj}^\pm is the field where layer j switches with the creation (+) or annihilation (-) of the wall, the expression for these switching fields becomes

$$H_{tj}^\pm = H_{cj} \pm \sigma_w / (2t_j M_{sj}). \quad (3)$$

As mentioned earlier, another possible kind of magnetization reversal process (see Fig. 3) is the case of simultaneous reversal of both layers when their TM moments (and, consequently, the RE ones) are parallel in the whole sample, without the creation of the wall across the thickness. From Eq. (2), the switching field for this case in the type-A ECDL (H_{t12A}) can be expressed as

$$H_{t12A} = (t_1 M_{s1} H_{c1} + t_2 M_{s2} H_{c2}) / |t_1 M_{s1} - t_2 M_{s2}|, \quad (4)$$

while, for the type-P ECDL, H_{t12P} can be written as

$$H_{t12P} = (t_1 M_{s1} H_{c1} + t_2 M_{s2} H_{c2}) / (t_1 M_{s1} + t_2 M_{s2}). \quad (5)$$

The first consequence that can be derived from these equations, in particular from Eq. (3), is that the effective switching field of each individual layer (H_{tj}) differs from its intrinsic coercivity (H_{cj}) by an amount $\pm \sigma_w / (2t_j M_{sj})$. Thus, this term can be understood as an exchange bias field $H_{\text{bias}} = \sigma_w / (2t_j M_{sj})$. Then, to compare with the experimental results, it is convenient to write it [in accordance with Eq. (3)] as

$$H_{\text{bias}} = (H_{tj}^- - H_{tj}^+) / 2. \quad (6)$$

Figure 4 presents the behavior of the H_{bias} field deduced from the hysteresis loops measured at the layer 1 side, following Eq. (6) and as indicated in the inset of the figure, in the temperature range just over T_{comp1} where the ECDL is type A and the loops present clear complete jumps at the switching fields (see Fig. 2, where some of the loops measured within this temperature interval are shown). The data are fitted to $H_{\text{bias}} = \sigma_w / (2t_1 M_{s1})$ considering the temperature dependence of the saturation magnetization of $\text{Gd}_x\text{Co}_{1-x}$ mentioned earlier, so that the energy per unit area of the wall at the ECDL interface divided by the thickness of the reversed layer can be obtained: $\sigma_w / t_1 = 4.1 \times 10^4 \text{ erg/cm}^3$. Although the effective thickness of the reversed layer cannot be strictly known due to the actual presence of the wall, it should be of the order of each layer thickness and, thus,

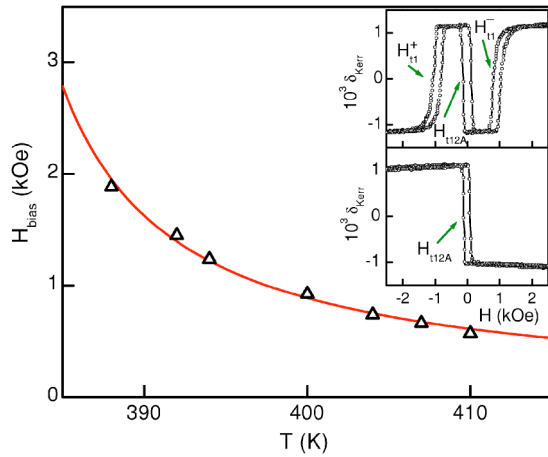


FIG. 4. (Color online) Temperature dependence of the H_{bias} field (symbols) deduced according with Eq. (6) from the switching fields observed in the TMOKE loops of the layer 1 side, that are indicated in the inset for the $T=400$ K case. The curve is a fit to the temperature dependence of $H_{bias} = \sigma_w / (2t_1 M_{s1})$.

$\sigma_w \approx 0.4$ erg/cm² can be estimated; this is a reasonable value as it is comparable with the one evaluated as $\sigma_w \approx (AK)^{1/2}$, A being the exchange constant and K the anisotropy energy. Once the value of σ_w/t_1 has been deduced it can be used, together with the earlier mentioned temperature dependences of the saturation magnetization and of the coercive field of the individual Gd_xCo_{1-x} layers, to calculate the temperature dependence of the different observed switching fields with the model of equations (3)–(5). In particular, Fig. 5 shows the comparison between the experimental data and these modeled fields in the range where the ECDL is type A with reversal processes dominated by the bottom layer and well-

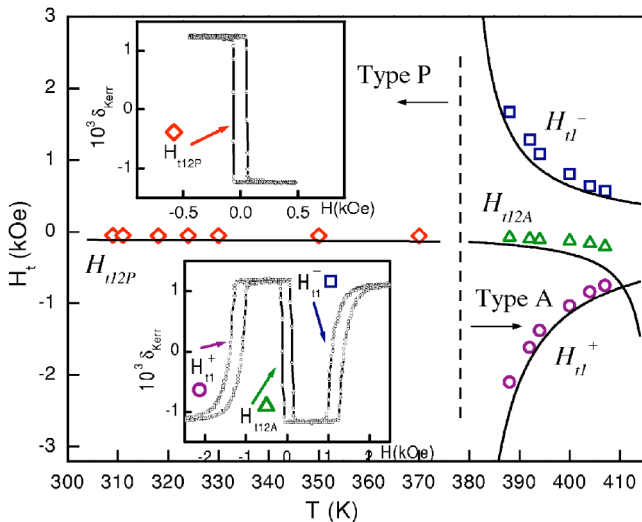


FIG. 5. (Color online) A comparison between the experimentally observed switching fields in the $Gd_{0.22}Co_{0.78}/Gd_{0.24}Co_{0.76}$ ECDL and the corresponding modeled temperature dependences of these fields. Each switching field is marked with a different symbol as indicated in the insets that correspond to loops measured from the layer 1 side at 330 K (type-P ECDL, top inset) and 394 K (type-A ECDL, bottom inset).

defined complete jumps in the TMOKE loops, that is $T < 410$ K, as well as in the type-P interval (see Fig. 2 to find some of the measured loops for both kinds of temperature intervals); the agreement between the model and the experiment (without any kind of further fitting) is quite well.

Moreover, the whole temperature dependence of all the possible switching fields involved in the magnetization reversal in the ECDL (see Fig. 3) can be modeled in the same way. Figure 6 represents the complete H - T phase diagram deduced from Eqs. (3)–(5) of H_{tj}^{\pm} , H_{t12A} , and H_{t12P} fields, using the known temperature dependences of M_{sj} and H_{cj} and the deduced energy term of the 180° Bloch wall at the interface. This diagram reveals the kind and sequence of the reversal processes that take place when the field is varied from positive to negative values in a hysteresis loop. For example, at $T=400$ K (i.e., for a type-A ECDL case and relatively close to one of the compensation temperatures), when reducing the field from positive saturation, the H_{t1}^- curve is first encountered, so that layer 1 is switched and the wall eliminated; then, the H_{t2}^- line is crossed, however, this reversal process cannot take place at this point as the wall has already been annihilated; by further decreasing the field and reversing its sign, H_{t12A} is reached, resulting in the simultaneous switching of both layers (M_{s2} is now parallel to H while M_{s1} is antiparallel); finally, the negative saturation is obtained at H_{t1}^+ where the wall is created by the reversal of layer 1. This sequence in the magnetization reversal process is actually what is observed in the TMOKE loops at this temperature range and corresponds to one of those sketched in Fig. 3(b) (the one with the sequence of states I—II—III—IV). Also, for the type-P ECDL case (for example, $T=370$ K), the H - T diagram indicates that, when varying the field from positive to negative saturation, both H_{t1}^- and H_{t2}^- lines are first reached but, as there is no wall at saturation to be annihilated none of these switching processes can take place [see Fig. 3(a)]; therefore, as it is observed experimentally in the TMOKE loops, the complete magnetization reversal process of the ECDL is obtained by the simultaneous switching of both layers when the H_{t12A} line is crossed. On the other hand, in the central region of the temperature interval between both compensation temperatures (that is, from about $T=408$ K to 431 K), the H - T phase diagram indicates the presence of different reversal processes, as there are some intersections between H_{tj}^{\pm} curves as well as a divergence in H_{t12A} (see Fig. 6). In particular, when decreasing the field at $T=420$ K the intersection point of H_{t1}^- and H_{t2}^- lines is found, so that the 180° Bloch wall across the thickness could be eliminated through two energetically equivalent reversal processes. In the following it will be shown that, associated with this intersection, a very stable magnetic configuration has been found in this kind of ECDL.

C. Double antiferromagnetic state

Figure 7 shows the detailed TMOKE hysteresis loops obtained by measuring from top and bottom sides of the bilayer [Fig. 7(a) and 7(b), respectively] illuminating the whole sample area at $T=420$ K (it is a detailed representation of the loops already shown in Fig. 2 for this temperature). As the

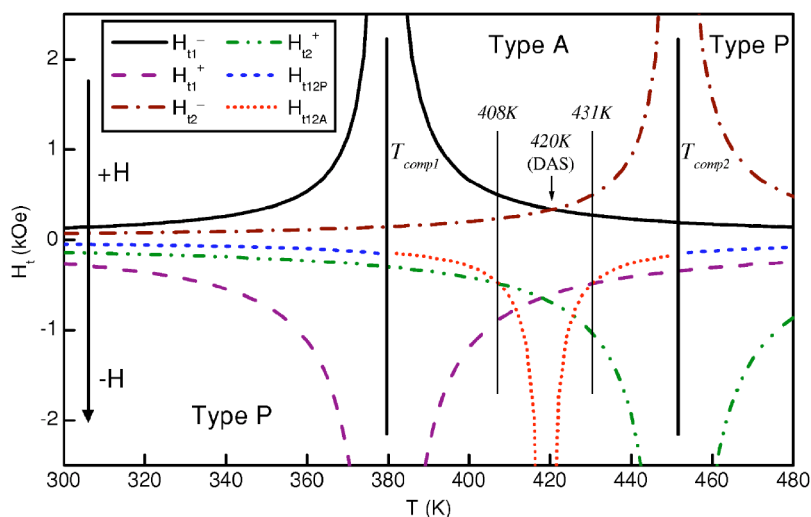


FIG. 6. (Color online) Complete H - T phase diagram of the different switching fields of the layers in the $\text{Gd}_{0.22}\text{Co}_{0.78}/\text{Gd}_{0.24}\text{Co}_{0.76}$ ECDL. The DAS state is indicated.

field is decreased from saturation, clear plateaus in the magnetization reversal process are observed in both hysteresis loops in a wide field interval (≈ 500 Oe) around remanence, indicating the presence of a very stable magnetization configuration at $H=0$. It is worthwhile to note that, at this plateau, the TMOKE signal is zero in both loops, which reveals a simultaneous zero net magnetization in the applied field direction within each layer. As discussed earlier, these results are very different from those observed in the other temperature ranges where the loops showed complete jumps at the switching fields, and, as both loops present jumps at similar field values, they seem to indicate that the magnetization reversal takes place through a first simultaneous switching in both layers at the respective H_{ij}^- fields to annihilate the wall across the thickness and reach the new stable state, followed by a second simultaneous reversal in both layers when H is varied further to create the wall at H_{ij}^+ .

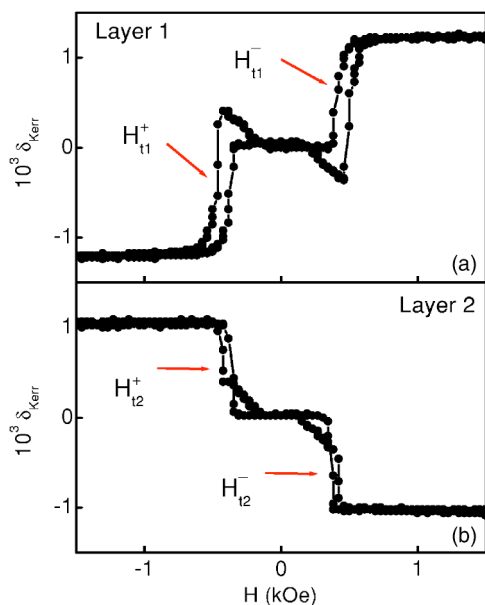


FIG. 7. (Color online) TMOKE loops measured illuminating the whole $\text{Gd}_{0.22}\text{Co}_{0.78}/\text{Gd}_{0.24}\text{Co}_{0.76}$ sample from (a) top and (b) bottom layer sides at $T=420$ K.

To explore the stable magnetization configuration associated with the plateau observed in the loops, TMOKE measurements have also been performed in several points along each side of the bilayer using a focused laser beam with a $500\text{ }\mu\text{m}$ -diameter spot. The results reveal a completely different behavior of the left and right regions within each $\text{Gd}_x\text{Co}_{1-x}$ layer as shown in Figs. 8(a)–8(d). Thus, while the hysteresis loop measured in a point of the left region of the top layer shows the characteristic easy axis behavior (with a

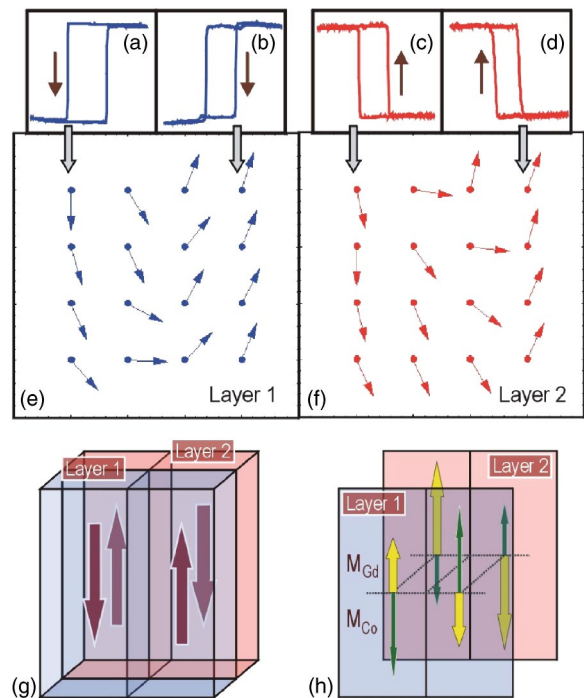


FIG. 8. (Color online) TMOKE loops (at $T=420$ K) measured focusing a laser on the (a) left and (b) right sides of the top layer, and the (c) left and (d) right sides of the bottom layer of the $\text{Gd}_{0.22}\text{Co}_{0.78}/\text{Gd}_{0.24}\text{Co}_{0.76}$ ECDL. The approximated configuration of the Co moments at $H=0$, deduced from the hysteresis loops obtained at 16 points, is represented for the (e) top layer and (f) bottom layer. Sketches of this state (DAS) for (g) the net magnetization and (h) the magnetic moments are also shown.

sharp jump at the coercive field from positive to negative saturation as the field is reversed to negative values [Fig. 8(a)], the loop measured in the right region of the same layer also presents a complete sharp jump in the magnetization reversal but at positive fields [Fig. 8(b)], so that the reduced remanence is $m_r \approx -1$. The opposite is observed in the hysteresis loops obtained in the bottom layer as the magnetization reverses at negative field values in the right region and at positive values at the left side. These results indicate the presence of a 180° magnetic domain wall across the width of the layers at remanence, that is, where the plateaus were detected in the hysteresis loops performed illuminating the complete layer. The configuration of this domain wall has been analyzed by measuring TMOKE loops in 16 points of each layer with the focused laser light (it is important to mention that the direct sum of the 16 loops in each layer produces a hysteresis loop that resembles in good approximation the one obtained illuminating the complete sample surface and shown in Fig. 7). As the bilayer does not show any significant magnetic anisotropy term in the direction perpendicular to the sample plane and, also, the measured loops present a smooth variation with the spot position, an in-plane uniform magnetization within each point has been considered in order to deduce the moments direction from the value of the Kerr signal at $H=0$; thus, the obtained Co magnetic moments configuration of the whole sample at remanence is represented in Figs. 8(e) and 8(f). These results actually show a very similar configuration of the Co magnetic moments (and therefore of the Gd ones) in the top and bottom layers, with moments in the left and right regions pointing in opposite directions along the easy axis and separated by a broad Neel-like wall (extended over a distance in the millimeter range) where the Co moments rotate in the same sense in the two layers (counterclockwise) from one sign to the other. It reveals that, to reduce the exchange energy associated with the wall across the thickness present in the saturation, half of each layer reverses its sign, reaching a configuration where that wall across the thickness is eliminated: the Co moments of both layers are now parallel in each point of the sample, according to the strong $3d$ - $3d$ exchange interaction at the interface. (It is worth remarking that the opposite configuration of the magnetic moments in the left and right regions is independent of the assumption of a uniform in-plane magnetization within each measured point, which only could affect the quantitative particular characteristics of the wall that separates both regions.)

This magnetic configuration state is sketched in Figs. 8(g) and 8(h) where the saturation magnetization and magnetic moments of each region are represented. Therefore, the $\text{Gd}_x\text{Co}_{1-x}/\text{Gd}_y\text{Co}_{1-y}$ bilayer actually presents a double antiferromagnetic state (DAS) configuration as, at a macroscopic level, the sample is generically divided in four regions so that the magnetization in each of them is antiparallely aligned to its immediate neighbors in thickness and width; it takes place while also, at a microscopic level and within each region, Gd and Co moments are antiferromagnetically coupled to each other. It is worthwhile to note that this DAS

configuration is very stable for several reasons; first, as the thicknesses and the saturation magnetizations of both layers are of a similar magnitude, the magnetostatic energy associated with the magnetic poles at the edges of the sample becomes strongly reduced due to the top-bottom closing of the stray fields; also, any further in-plane wall movement to completely reverse the magnetization in the top layer is reciprocally blocked with the one of the bottom layer as their moments rotate in opposite directions (and it implies the creation of the wall across the thickness). It is in good agreement with the plateaus observed in the loops over a wide field range of 500 Oe. From a phenomenological point of view, the observed field induced transition from a magnetic state with low net magnetization to another with high magnetization (as those present in the loops of Fig. 7), in both cases with small susceptibility, is similar to the spin-flip metamagnetic transition observed in antiferromagnetic materials with high uniaxial anisotropy.²⁶ In the present case, it is the energy associated with the creation of a wall across the thickness and the domain structure (and not the anisotropy energy) which drives the process.

As suggested before, the presence of this DAS configuration can also be understood in terms of the deduced H - T phase diagram shown in Fig. 6. Thus, when decreasing the field at $T=420$ K the intersection point of H_{i1}^- and H_{i2}^- lines is found; it actually results in the experimentally observed DAS configuration, where each half of the bilayer switches via these two modes to eliminate the wall at the ECDL interface. Then, the DAS configuration remains stable until the field reaches the H_{ij}^+ curves several hundred oersted further, in good agreement with the plateaus observed in the hysteresis loops.

IV. CONCLUSIONS

In summary, magneto-optical hysteresis loops measured from both sides of the samples have shown a rich variety of behaviors in the magnetization reversal processes of exchange coupled $\text{Gd}_x\text{Co}_{1-x}/\text{Gd}_y\text{Co}_{1-y}$ bilayers in the temperature interval where the saturation magnetizations of both layers are of comparable magnitude. The whole observed behavior can be understood in terms of a deduced general H - T phase diagram, than can also be applied to describe and predict the magnetization states in other similar magnetic systems. Moreover, a double antiferromagnetic configuration has been found at temperatures between the compensation temperatures of both layers. This magnetization state is very stable (over a wide field interval of ≈ 500 Oe), and it is separated from the saturation by a field induced transition that presents the phenomenological characteristics of a macroscopic spin-flip metamagnetic transition.

ACKNOWLEDGMENTS

This work was supported by Spanish CICYT (Grant No. MAT2002-04543-C02-01). We acknowledge useful discussions with J. L. Vicent and F. Briones.

*Electronic address: jmartin@condmat1.ciencias.uniovi.es

- ¹P. Grünberg, R. Schreiber, Y. Pang, M. B. Brodsky, and H. Sowers, Phys. Rev. Lett. **57**, 2442 (1986).
- ²M. N. Baibich, J. M. Broto, A. Fert, F. Nguyen Van Dau, F. Petroff, P. Etienne, G. Creuzet, A. Friederich, and J. Chazelas, Phys. Rev. Lett. **61**, 2472 (1988).
- ³S. S. P. Parkin, N. More, and K. P. Roche, Phys. Rev. Lett. **64**, 2304 (1990).
- ⁴D. J. Monsma, J. C. Lodder, Th. J. A. Popma, and B. Dieny, Phys. Rev. Lett. **74**, 5260 (1995).
- ⁵M. D. Stiles, J. Magn. Magn. Mater. **200**, 322 (1999), and references therein.
- ⁶B. Heinrich, Y. Tserkovnyak, G. Woltersdorf, A. Brataas, R. Urban, and G. E. W. Bauer, Phys. Rev. Lett. **90**, 187601 (2003).
- ⁷J. Nogués and I. K. Schuller, J. Magn. Magn. Mater. **192**, 203 (1999), and references therein; C. Leighton, M. R. Fitzsimmons, P. Yashar, A. Hoffmann, J. Nogués, J. Dura, C. F. Majkrzak, and I. K. Schuller, Phys. Rev. Lett. **86**, 4394 (2001).
- ⁸D. Haskel, G. Srajer, J. C. Lang, J. Pollmann, C. S. Nelson, J. S. Jiang, and S. D. Bader, Phys. Rev. Lett. **87**, 207201 (2001).
- ⁹S. M. Valvidares, L. M. Álvarez-Prado, J. I. Martín, and J. M. Alameda, Phys. Rev. B **64**, 134423 (2001).
- ¹⁰J. L. Leal and M. H. Kryder, J. Appl. Phys. **83**, 3720 (1998).
- ¹¹Z. S. Shan, D. J. Sellmyer, S. S. Jaswal, Y. J. Wang, and J. X. Shen, Phys. Rev. Lett. **63**, 449 (1989).
- ¹²S. S. Yan, R. Schreiber, F. Voges, C. Osthöver, and P. Grünberg, Phys. Rev. B **59**, R11 641 (1999).
- ¹³V. K. Vlasko-Vlasov, U. Welp, J. S. Jiang, D. J. Miller, G. W. Crabtree, and S. D. Bader, Phys. Rev. Lett. **86**, 4386 (2001).
- ¹⁴P. Hansen, in *Handbook of Magnetic Materials*, edited by K. H. J. Buschow (Elsevier, Amsterdam, 1991), Vol. 6, p. 289.
- ¹⁵T. Kobayashi and H. Tsuji, Jpn. J. Appl. Phys. **20**, 2089 (1981).
- ¹⁶B. Dieny, D. Givord, J. M. B. Ndjaka, and J. M. Alameda, J. Appl. Phys. **67**, 5677 (1990).
- ¹⁷P. Chaudhari, J. J. Cuomo, and R. J. Gambino, Appl. Phys. Lett. **22**, 337 (1973).
- ¹⁸H. Fu, M. Mansuripur, and P. Meystre, Phys. Rev. Lett. **66**, 1086 (1991).
- ¹⁹D. Raasch and H. Wierenga, J. Magn. Magn. Mater. **168**, 336 (1997).
- ²⁰T. Fukami, Y. Nakaki, T. Tokunaga, M. Taguchi, and K. Tsutsumi, J. Appl. Phys. **67**, 4415 (1990).
- ²¹K. Röhl, in *Magnetic Multilayers and Giant Magnetoresistance*, edited by U. Hartmann (Springer-Verlag, Berlin, 2000), p. 13, and references therein.
- ²²R. Morales and J. M. Alameda, IEEE Trans. Magn. **37**, 2305 (2001).
- ²³C. Dehesa-Martínez, L. Blanco-Gutiérrez, M. Vélez, J. Díaz, L. M. Alvarez-Prado, and J. M. Alameda, Phys. Rev. B **64**, 024417 (2001).
- ²⁴D. Mergel, J. Appl. Phys. **74**, 4072 (1993).
- ²⁵D. Givord, J. Betz, K. Mackay, J. C. Toussaint, J. Voiron, and S. Wüchner, J. Magn. Magn. Mater. **159**, 71 (1996); T. Yonamine, A. P. B. Tufaille, A. D. Santos, and Y. Souche, J. Appl. Phys. **81**, 5722 (1997).
- ²⁶E. Strykowski and N. Giordano, Adv. Phys. **26**, 487 (1977).